New Unsaturated Erosion Model for Landslide: Effects of Flow Particle Size and Debunking the Importance of Frictional Stress

Author 1

- Clarence Edward Choi, Assistant professor
- Department of Civil Engineering, The University of Hong Kong, Hong Kong SAR, China
- ORCID: https://orcid.org/0000-0002-9712-1524
- Email: cechoi@hku.hk

Author 2

- Pengjia Song, PhD student
- Department of Civil Engineering, The University of Hong Kong, Hong Kong SAR, China
- ORCID: https://orcid.org/0000-0001-9945-5344
- Email: songpj@connect.hku.hk

Corresponding author:

Pengjia Song, PhD student

Department of Civil Engineering, The University of Hong Kong, Hong Kong SAR, China

ORCID: https://orcid.org/0000-0001-9945-5344

Email: songpj@connect.hku.hk

Abstract

Flow-type landslides, such as debris flows and rock avalanches, erode soil bed material as they flow downslope. The eroded material increases the volume of a landslide, and thus, its destructive potential. Among existing erosion theories, it remains unclear whether frictional or collisional shear stresses govern the erosion process. Moreover, existing theories do not consider the flow basal slip condition on the erosion dynamics at the flow-bed interface, nor do they consider the effects of volumetric response on the shear strength of unsaturated soil beds. In this study, an erosion model that considers the effects of basal slip condition and the volumetric response of unsaturated soil beds is proposed and evaluated with a unique set of experiments. Boundary collisional stresses drive soil bed erosion, while boundary frictional shear stresses are counteracted by the soil strength mobilized by overburden induced volume contraction. The flow particle size and Froude number are shown to be adequate indicators of the of the boundary collisional stresses that govern the erosion rate. Findings from this study hint at the conjecture that existing erosion models may not be equipped with the necessary physics to provide realistic hazard assessments of flow-type landslides eroding soil beds.
Keywords: Landslides; Soil bed erosion; Physical modelling; unsaturated soil;

1. INTRODUCTION

Flow-type landslides (Hungr *et al*., 2014) are masses of geomaterial that flow downslope under the influence of gravity. They erode soil and rock bed material along the flow path (Jerolmack & Daniels, 2019). Erosion increases the size of flow-type landslides, resulting in longer runout distances and greater destructive potential (e.g., Hungr & Evans, 2004). Evidently, advancing the current understanding of the mechanisms of erosion by flow-type landslides is crucial for improving vulnerability assessments to safeguard human life and infrastructure in mountainous regions globally.

The most important aspect of erosion modelling is describing the driving mechanism that causes soil bed failure. Existing theories mainly propose that soil bed erosion is driven by frictional shear stress τ_f at the flow-bed interface (Takahashi, 1978; McDougall & Hungr, 2005; Pirulli & Pastor 2012)):

$$\tau_\mathrm{f} = \sigma_\mathrm{n}\tan\phi_\mathrm{i}{}' = \rho_\mathrm{f}\mathrm{g}h_\mathrm{f}\cos\alpha\tan\phi_\mathrm{i}{}' \quad (1)$$

where σ_n is the normal stress induced by the flow overburden, $\phi_\mathrm{i}{}'$ is the interface friction angle between the flow and the bed, ρ_f is the bulk flow density, g is the gravitational acceleration, h_f is the flow depth and α is the slope. The frictional shear stress induced by flow overburden is assumed to act uniformly on a soil bed. In turn, erosion occurs when the frictional shear stress exceeds the soil bed strength. Field measurements from Illgraben, Switzerland, hinted at the conjecture that soil bed erosion mainly occurred during the passage of the bouldery and collisional flow front. During the passage of the flow front, the measured frictional shear stress was smaller than the soil bed strength (Berger et al., 2012). But interesting, erosion still occurred. This implies that another erosion mechanism besides frictional shear stress must be driving the erosion process. Based on this important field observation, Song & Choi (2021) carried out an experimental investigation to demonstrate that collisional stresses σ_c (Bagnold, 1954) at the front of flow-type landslides play an important role in soil bed erosion:

$$\sigma_\mathrm{c} = \nu_\mathrm{f}\rho_\mathrm{s}\dot{\gamma}^2 D^2 \quad (2)$$

where ν_f is the solid volume fraction of the flow, ρ_s is the density of the flow particles, $\dot{\gamma}$ is the shear rate defined as the velocity gradient normal to the bed, and D is the characteristic flow particle size. Equation (2) shows that the flow particle size governs the magnitude of the collisional stresses and flow dynamics. Boundary collisional stress can be viewed as the sum of the point loads acting over a unit area. Collisional stress serves as an indicator of the magnitude of the point loads imposed by flow particles on a soil beds. It is worthwhile to note that point loads act over a small contact area such that they can be several orders of magnitudes larger than the collisional stresses calculated by using Equation (2).

Erosion induced by collisional stresses can be assessed based on the basal slip velocity, which is the flow velocity at the flow-bed interface (Artoni *et al.*, 2012). The velocity of the particles adjacent to the soil

bed increases with basal slip velocity, which increases the collisional impact forces imposed on a soil bed. A small or zero basal slip velocity means that the flow particles at the soil bed will come to rest and deposit. The deposited material will then shield the bed from further erosion (Sklar & Dietrich, 2001; Song & Choi, 2021). Despite the importance of the basal slip velocity, existing formulation (i.e., equation 2) does not consider it. Equation (2) only describes the inter-particle collisional stresses within the flow (Bagnold, 1954) instead of those at the flow-bed interface (i.e., the boundary collisional stresses). Thus, the expression of boundary collisional stresses by considering the basal slip velocity is necessary for evaluating the soil bed erosion driven by collisional stresses.

Savage and Hutter (1989) introduced the Savage number N_{Sav}, which is defined as the ratio of the collisional to frictional shear stresses:

$$N_{\mathrm{Sav}} = \frac{\nu_{\mathrm{f}}\rho_{\mathrm{s}}\dot{\gamma}^2 D^2}{\rho_{\mathrm{f}} g h_{\mathrm{f}} \cos\alpha \tan\phi_{\mathrm{i}}'} \quad (3)$$

Collisional stresses dominate the flow dynamics as well as soil bed erosion when the Savage number is larger than 0.1. Otherwise, frictional shear stress dominates. In the field, the flow particle size can span six orders of magnitude from 10^{-4} to 10^{2} m (Iverson, 1997). In turn, the boundary stresses that drive erosion are strongly influenced by the particle size. Notwithstanding, in the experiments of Song & Choi (2021), only a single particle size that enabled collision dominated flows was modelled. Consequently, the competing effects between frictional and collisional stresses on soil bed erosion could not be revealed.

Another area of deficiency in existing theories of erosion by flow-type landslides is neglecting the effects of the volumetric response of the soil bed on its strength. Existing theories (Takahashi, 1978; McDougall & Hungr, 2005) assume that the soil beds are fully saturated when erosion occurs, and the soil volume remains constant when subjected to the rapid undrained landslide loading. The landslide loading results in the increase of pore water pressure, which in turn decreases the effective stress and the strength of the soil bed. However, soil beds are rarely fully saturated in nature (McCoy *et al.*, 2012). When subjected to the rapid undrained landslide loading, the volume of unsaturated soil contracts due to the large compressibility of pore air. In turn, compression enhances the effective stress, and thus the soil strength. It is expected that the soil strength mobilized by the overburden of a flow will weaken the role played by frictional shear stress on soil bed erosion. However, the aforementioned effect has yet to be evaluated.

In this study, the competing effects between boundary collisional stresses and the frictional shear stress in soil bed erosion is examined by conducting a unique series of experiments by varying the particle size of experimental flows travelling over unsaturated soil beds. A new erosion model, which considers the boundary collisional stresses, is proposed and evaluated using the said experimental data.

2. A NEW THEORETICAL MODEL OF BED EROSION BY BOUNDARY COLLISIONAL STRESSES

In this section, the boundary collisional stresses, which consider the basal slip velocity, and the unsaturated soil bed strength, which considers the effects of soil volume contraction under landslide loading, are discussed. These additional considerations are advancements over the erosion model proposed by Song and Choi (2021). Then, the driving and resisting mechanisms are used to quantify the erosion potential of flow-type landslides.

2.1 Boundary collisional stresses at the flow-bed interface

Collisional stresses are defined as the sum of the instantaneous contact forces applied over a unit area (Bagnold, 1954). Therefore, the boundary collisional stresses can be calculated as the product of the impact force generated by a single flow particle Γ, number of particles in a unit area n, and the frequency $\dot{\gamma}$ of each particle colliding with the soil bed.

To deduce the scaling relationship between a particle and the impact force that it exerts on the soil bed, we assume that particles impact the soil bed at the same velocity as the basal slip velocity u_{sl}. Yohannes *et al.* (2012) carried out theoretical analysis and numerical modelling based on the Hertzian contact mechanics to investigate the impact force by a single particle on a rigid plane. It was proposed that the impact force Γ scales proportionally to the mass of the particle and exhibits a power-law dependence on the impact velocity u_{sl}:

$$\Gamma \propto \frac{\pi D^3}{6}\rho_{\mathrm{s}} u_{\mathrm{sl}}^{k} \tag{4}$$

where k is a constant. The number of particles in a unit area can be calculated as the ratio of the solid volume fraction of the flow ν_{f} to the square of the particle size D (Bangnold, 1954):

$$n = \frac{\nu_{\mathrm{f}}}{D^2} \tag{5}$$

The basal shear rate $\dot{\gamma}$ describes the collision frequency between flow particle and the bed, and is correlated to the boundary collisional stresses that are induced on the bed. Therefore, it is assumed that the dependence of basal boundary collisional stresses on the shear rate $\dot{\gamma}$ conforms to a power-law relationship with a power-law coefficient of k (Farin *et al.*, 2019). The basal boundary collisional stresses σ_{bc} can be calculated as follows:

$$\sigma_{\mathrm{bc}} = \xi \nu_{\mathrm{f}} \rho_{\mathrm{s}} D (\dot{\gamma} u_{\mathrm{sl}})^{k} \tag{6}$$

where ξ is a constant with a dimension of $(m/s^2)^{1-k}$ to ensure the right side of the equation has the same dimension with stress.

Furthermore, two assumptions are required to link the shear rate $\dot{\gamma}$ and basal slip velocity u_{sl} to the bulk flow properties (i.e., mean flow velocity $\bar{u}$ and flow height h_{f}). First, the velocity profile is assumed to be linear with a basal slip velocity u_{sl}. The shear rate $\dot{\gamma}$ can then be calculated as follows:

$$\dot{\gamma} = \frac{u_{\mathrm{su}} - u_{\mathrm{sl}}}{h_{\mathrm{f}}} = \frac{2\bar{u} - 2u_{\mathrm{sl}}}{h_{\mathrm{f}}} \tag{7}$$

where u_{su} is the velocity at the flow surface. Secondly, u_{sl} and $\dot{\gamma}$ conform to the following relationship:

$$\frac{u_{\mathrm{sl}}}{\dot{\gamma} h_{\mathrm{f}}} = \beta \tag{8}$$

where β is a constant determined based on the flow basal resistance. Equation (8) was proposed by Artoni *et al.* (2012) based on regression analysis of discrete element simulation results, which modelled slight poly-dispersed granular flows down an inclined channel with different basal resistances. Combining equations (7) and (8) yields:

$$\dot{\gamma} = \frac{2\bar{u}}{(1+2\beta)h_{\mathrm{f}}} \tag{9a}$$

$$u_{\mathrm{sl}} = \frac{2\beta\bar{u}}{1+2\beta} \tag{9b}$$

Substituting equation (9) into equation (6) yields:

$$\sigma_{\mathrm{bc}} = \xi \mathrm{g}^k \left[\frac{4\beta}{(1+2\beta)^2}\right]^k \nu_{\mathrm{f}} \rho_{\mathrm{s}} D \left(\frac{\bar{u}}{\sqrt{g h_{\mathrm{f}}}}\right)^{2k} \tag{10}$$

The term $\xi \mathrm{g}^k \left[\frac{4\beta}{(1+2\beta)^2}\right]^k$ has the same dimensions as acceleration and can be substituted with $\chi \mathrm{g}$, where χ is a dimensionless coefficient related to the basal resistance. Equation (10) can then be rewritten as:

$$\sigma_{\mathrm{bc}} = \chi \mathrm{g} \nu_{\mathrm{f}} \rho_{\mathrm{s}} D Fr^{2k} \tag{11a}$$

$$Fr = \frac{\bar{u}}{\sqrt{\mathrm{g} h_{\mathrm{f}}}} \tag{11b}$$

where Fr is the Froude number. It is evident from equation (11) that the boundary collisional stresses are governed by the Froude number and the flow particle size.

2.2 Unsaturated Soil bed strength and debunking the importance of frictional shear stress in soil bed erosion

The volumetric response of soil subjected to undrained loading significantly influences the soil strength by regulating the loading taken by the solid skeleton (i.e., the effective stress) (Fredlund *et al.*, 1978). Flow-type landslides travel at high speeds and induce rapid loading on the soil bed (Hungr *et al.*, 2014), and the soil bed is subjected to undrained shearing (Iverson, 2012) where load from the overriding landslide is simultaneously sustained by the pore fluid and the soil skeleton due to the large compressibility of the pore air. The increase of effective stress $\Delta(\sigma_{\mathrm{n}} - p_{\mathrm{a}})$ can be described as follows:

$$\Delta(\sigma_{\mathrm{n}} - p_{\mathrm{a}}) = (1 - B)\sigma_{\mathrm{n}} = (1 - B)\rho_{\mathrm{b}} g h_{\mathrm{f}} \cos\alpha \quad (12)$$

where B is the pore fluid pressure parameter, which describes the proportion of the flow overburden sustained by the pore fluids (Skempton, 1954). In fact, there are pore air pressure B_{a} and pore water pressure B_{w} to represent the proportion of loading sustained by the pore air and pore water. Hilf's analysis (Hilf, 1948) has demonstrated that satisfying results can be obtained by assuming $B_{\mathrm{a}} = B_{\mathrm{w}} = B$.

The strength of unsaturated soil subjected to rapid shearing by flow-type landslides can be expressed as follows:

$$\tau_{\mathrm{s}} = \sigma_0' \tan\phi' + (1 - B)\sigma_{\mathrm{n}} \tan\phi' + (p_{\mathrm{a}} - p_{\mathrm{w}}) S_{\mathrm{r}}^{\mathrm{m}} \tan\phi' \quad (13)$$

where p_{a} is the pore air pressure, p_{w} is the pore water pressure, $(p_{\mathrm{a}} - p_{\mathrm{w}})$ is the matric suction, ϕ' is the effective friction angle of the soil, σ_0' is the initial effective stress of the soil bed before erosion, S_{r} is the degree of saturation of a soil bed and m is a constant. The items on the right side of equation (13) represent the unsaturated soil strength contributed by the initial effective stress, flow overburden and the matric suction, respectively. Based on equation (13), the Factor of Safety (FoS) of an unsaturated soil bed subjected to the frictional shear stress only can be defined as:

$$FoS = \frac{\sigma_0' \tan\phi' + (1-B)\sigma_{\mathrm{n}} \tan\phi' + (p_{\mathrm{a}} - p_{\mathrm{w}}) S_{\mathrm{r}}^{\mathrm{m}} \tan\phi'}{\sigma_{\mathrm{n}} \tan\phi_{\mathrm{i}}'} \quad (14a)$$

$$FoS = \frac{\sigma_0' \tan\phi'}{\sigma_{\mathrm{n}} \tan\phi_{\mathrm{i}}'} + \frac{(1-B)\sigma_{\mathrm{n}} \tan\phi'}{\sigma_{\mathrm{n}} \tan\phi_{\mathrm{i}}'} + \frac{(p_{\mathrm{a}} - p_{\mathrm{w}}) S_{\mathrm{r}}^{\mathrm{m}} \tan\phi'}{\sigma_{\mathrm{n}} \tan\phi_{\mathrm{i}}'} \quad (14b)$$

where S_{r} is the normalized degree of saturation, m is a constant. The second item on the right side of equation (14b) (Noted as FoS_{ms}) represents the FoS determined by the soil strength mobilized by the flow overburden due to the volume contraction of the soil bed. A minimum value of FoS_{ms} can be calculated with parameters shown in Table 1, and the calculated FoS_{ms} are larger than unity.

Therefore, the frictional shear stress induced by flow-type landslides is normally totally counteracted by the unsaturated soil strength mobilized by the flow overburden and is theoretically insufficient to erode an unsaturated soil bed.

Table 1. Parameters adopted for the evaluation of the lower bound of FoS_m

Parameters	value	Reference
Interface friction angle, ϕ_i' (°)	9.7	McArdell et al. (2007); Berger et al. (2011)
Friction angle of the channel sediment, ϕ' (°)	15	GEO report No.325 (2017)
Maximum saturation of channel sediment, S_r(%)	90	Coe et al. (2008); McCoy et al. (2012)
Pore pressure parameter with the maximum saturation, B	0.3	Fredlund et al., 1993

2.3 Modified expression of the erosion potential of flow-type landslides

It is acknowledged that flow-type landslides impose both boundary collisional stresses and the frictional shear stress on the soil bed, but it is shown that frictional shear stress alone is insufficient to erode an unsaturated soil bed. Furthermore, soil beds are rarely fully saturated when landslides occur in nature. Therefore, the erosion potential of flow-type landslides can be defined solely by boundary collisional stresses. Following Song & Choi (2021), N_{SNCS} can be modified to N_C to characterize the erosion potential of flow-type landslides on a soil bed:

$$N_C = \frac{\sigma_{bc}}{\tau_s} = \frac{\chi g \nu_f \rho_s D Fr^{2k}}{[\sigma_0' + (1-B)\sigma_n]\tan\phi' + (p_a - p_w)\tan\phi^b} \quad (15)$$

The erosion potential of the flow-type landslides is proportional to the erosion rate of the soil bed.

3. PHYSICAL MODELLING OF SOIL BED EROSION

3.1 Configuration of the flume

To evaluate the proposed erosion model (equation (15)), a flume with a length of 3 meters and a width of 0.2 meter was used (Fig. 1(a)) to conduct experiments to simulate the erosion of a soil bed. The flume consists of a storage container with a pneumatic gate to store and release the source material, a rigid section to accelerate the flow and an erodible section to simulate the soil bed. The rigid section has a length of 1.45 m, and the erodible section has a length of 0.85 m and a depth of 72 mm.

3.2 Instruments

A force plate with a length, width, and thickness of 200 m, 50 mm, and 9 mm, respectively, is installed (Fig. 1(b)) at an inclined distance of 0.15 m upstream from the interface between the rigid and erodible sections. The force plate sits flush with the surface of the rigid channel bed. A load cell is installed underneath the force plate to measure the basal stresses induced by the model flows. In addition, an ultrasonic sensor, with a sampling rate of 2000 Hz, is mounted above the centre of the force plate to measure the flow depth. A high-speed camera, which has a sampling rate of 500 frames per second, is mounted at the side of the erodible section of the transparent acrylic side wall of the flume to capture the flow kinematics.

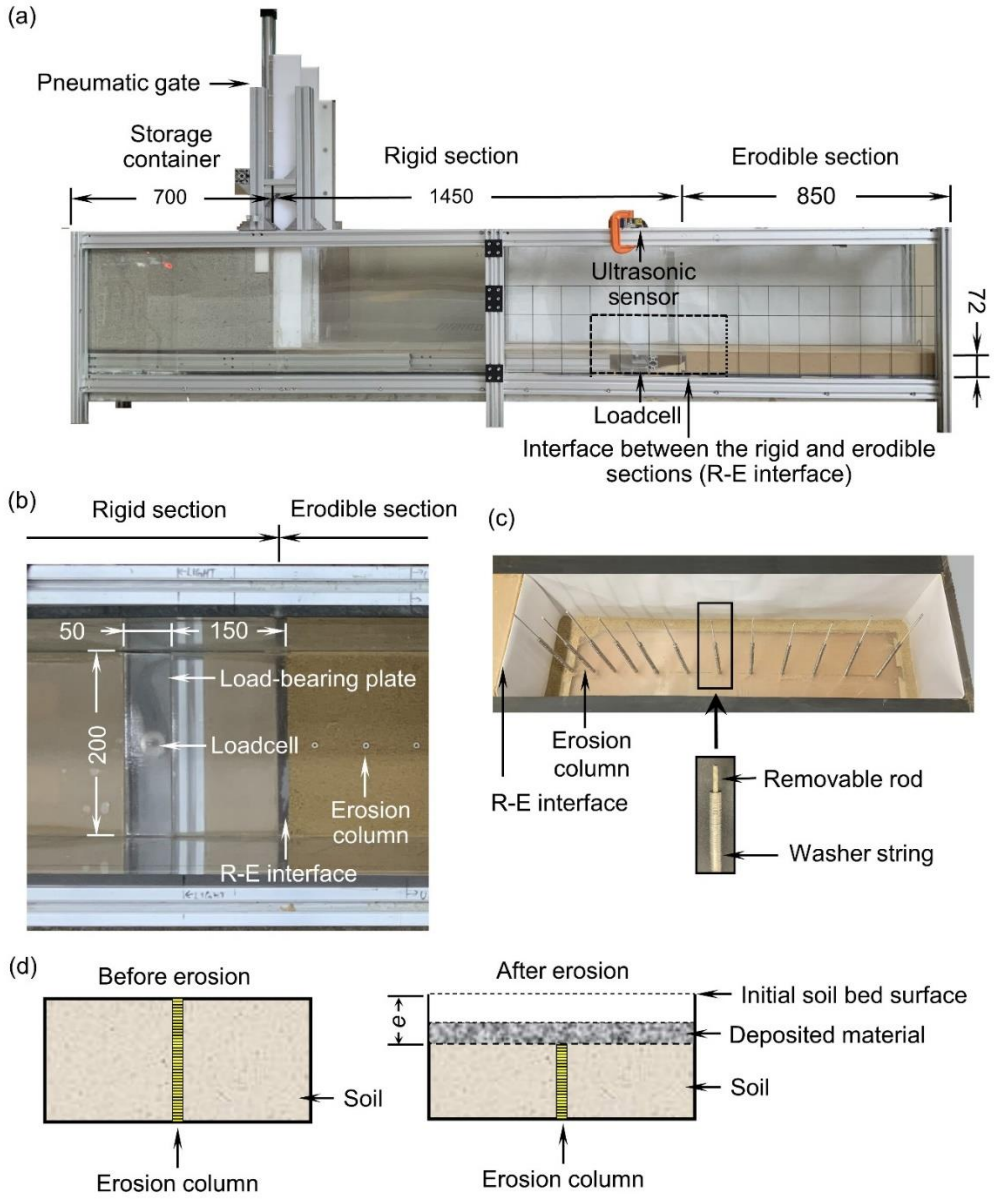

Figure 1. Experimental setup: (a) side view of the flume; (b) top view of the force-bearing plate and loadcell; (c) erosion columns at the base of the erodible bed without soil used in Song & Choi (2021)

(courtesy of the Journal of Geophysical Research: Earth Surface) and (d) Schematic illustration of the working principal of the erosion column. All dimensions are in millimetre.

A total of 14 erosion columns (Fig. 1(c)) were installed along the centreline of the erodible section to measure the erosion depth, which is often masked by the deposited material. The erosion columns are strings of washers, which are prepared to the same elevation as the soil bed before each experiment. The threaded rods are removed before the gravel flows are released down the channel. When the gravel flows over the erodible section, the washers are entrained with the eroded soil bed. The erosion depth is deduced based on the difference between the height of the erosion columns before and after each experiment (Fig. 1(d)).

Table 2. Test program and the properties of flow and bed material

Test ID	Grain size range, mm	Representative grain size, D: mm	Flow solid volume fraction, ν_f	Volumetric bed water content, θ: %	Bulk density of the erodible bed, ρ_{bed}: kg/m^3
F11D130B5	10 - 12	11	0.54	5	1464
F90D130B5	8 - 10	9	0.51	6	1438
F7D130B5	5 - 8	7	0.53	6	1464
F4D130B5	2.4 - 5	4	0.51	5	1472
F1.5D130B5	0.6 - 2.4	1.5	0.52	6	1430
F0.2D130B5	0.1 - 0.3	0.2	0.53	6	1472
F11D110B5	10 - 12	11	0.54	6	1413
F11D90B5	10 - 12	11	0.54	6	1481
F11D70B5	10 - 12	11	0.54	6	1430
F11D50B5	10 - 12	11	0.54	6	1455
F11D30B5	10 - 12	11	0.54	6	1455
F4D130B28	2.4 - 5	4	0.51	28	1667
F4D130B25	2.4 - 5	4	0.51	25	1650
F4D130B20	2.4 - 5	4	0.51	20	1565
F4D130B17	2.4 - 5	4	0.51	17	1599
F4D130B13	2.4 - 5	4	0.51	14	1523
F4D130B10	2.4 - 5	4	0.51	10	1523

3.3 Scaling consideration, test program and test procedures

Equation (15) reveals that the boundary collisional stresses as well as the erosion potential of the flow scales to the flow particle size and the flow Froude number. The prototype particle size typically ranges from 10^{-5} to 10^{1} m (Iverson, 1997) and the Froude number of typical flow-type landslides ranges from 0.4 to 7.6 (McArdell *et al.*, 2007; McCoy *et al.*, 2012; Kwan *et al.*, 2015; Zhou *et al.*, 2019). In this study, we model mono-disperse dry gravel flows composed of angular particles with different sizes from 10^{-4} to 10^{-2} m. The flows modelled in the experiments have a narrow range of grain size to minimize the effects of grain-size segregation (Zhou *et al.*, 2020). More importantly, dry granular flows are modelled to avoid scaling issues that arise from the interstitial fluid (Iverson, 2015). In this study, it is idealized that the erosion of soil bed mostly occurs during the passing of the highly-porous partially-saturated boulder-enriched flow front (Berger *et al.*, 2011), where the effects of the interstitial fluid are diminished. The

flow Froude number was varied by changing the length of the rigid section from 0.3 to 1.3 m. The strength of the soil bed is varied by changing its water content.

Before each experiment, the pneumatic gate is closed, and 70 kg of gravel is placed in the storage container to use up the storage capacity and maximize the erosion potential. Then, the erosion columns are installed. Afterwards, standard testing Toyoura sand is mixed uniformly with water to achieve the appropriate water content and then placed in the erodible section with a target dry density of 1400 kg/m^3 to ensure a representative dry density as that in the field (McCoy *et al.*, 2012). In each experiment, the flume is inclined to 34 degrees. The pneumatic gate is then opened to a height of 0.12 m to allow the gravel to discharge downslope and generate quasi-steady flows. A summary of the test program and the properties of the materials are given in Table 2.

4. RESULTS AND DISCUSSION

The flow velocity and erosion duration during each test can be deduced by the images captured by the high-speed camera. Flow depth is captured by the ultrasonic sensor and the erosion depth can be deduced with the erosion columns. A summary of the test results is shown in Tables 3 and 4. Typical flow kinematics captured by the high-speed camera on the erodible bed are shown for test F11D130B5 in the supporting information. It is evident from the Figure 2 that the flow particles adjacent to the soil bed decelerate when they override the soil bed. The particles deposit when their velocities reach zero and consequently shield the soil bed from erosion.

4.1 Boundary collisional stresses generated by flows with different particle sizes and Froude number

Figure 3 shows a typical time-history of the load measurements from the loadcell in test F11D130B5. The grey curve shows the denoised measurement of the basal force generated by the overriding flow by using the wavelet transform method (Lang *et al.*, 1996). The black curve shows the moving average of the basal force with a bin size of 100 samples. The moving average of the basal force represents load contribution from the flow overburden (McCoy *et al.*, 2013). The measured basal force fluctuates widely from its moving-average value after the arrival of the flow front ($t = 0$). Figure3 indicates that basal forces tend to be underestimated in existing theories because only the load contributed from the flow overburden (i.e., the black curve) is considered. Nevertheless, the basal force can be up to four times (in this study) or five times (field measurement obtained by McCoy *et al.*, 2013) larger than the overburden due to the collisions of flow particles with the bed.

The fluctuating component of the basal force can be analysed statistically to quantify the contribution of the basal collisional stresses (Hsu *et al.* 2014). The probability distribution of the normalized basal force, which is obtained by dividing the denoised basal force by its moving-average, in Figure 3 is calculated when a nearly steady mean basal force is measured (i.e., bracketed by the two vertical dash lines). When

the normalized basal force is unity, it means that the flow basal force is equivalent to the flow overburden pressure and the basal collisional stresses are negligible. By contrast, when the normalized basal force is larger than unity, it means that the boundary collisional stresses contribute to the flow basal force.

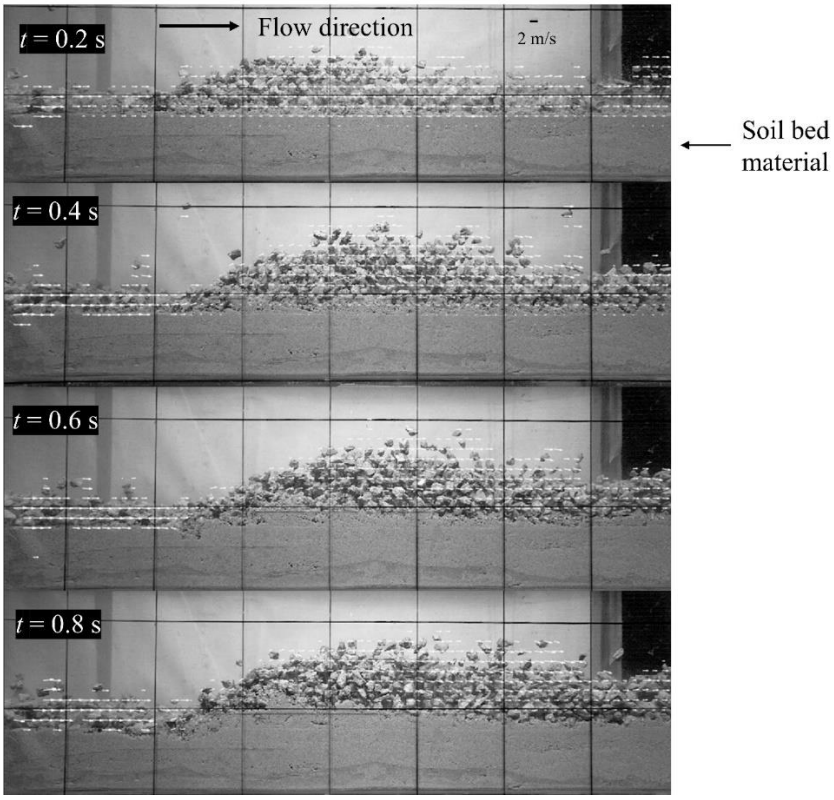

Figure 2. Flow kinematics captured by the high-speed camera since the flow reached the R-E interface (t = 0)

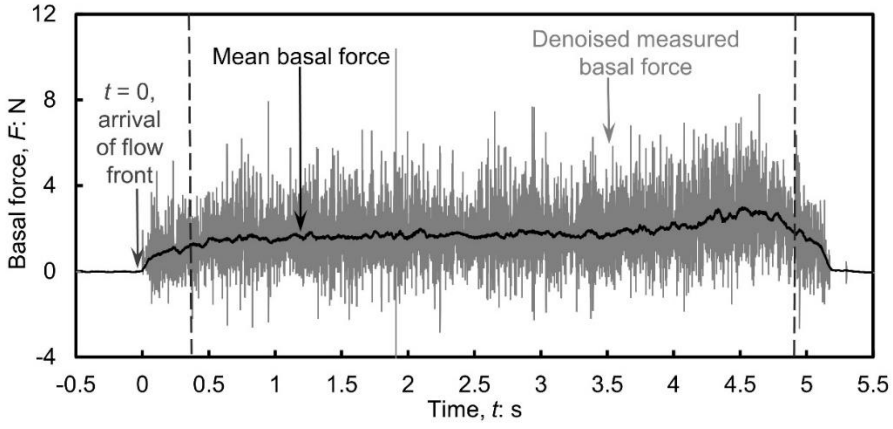

Figure 3. Time-history of a typical denoised basal forces and the moving-averaged basal forces measured by the loadcell in the test F11D130B5 (D = 11 mm, Fr = 6.7, θ = 5%)

The probability distribution of the normalized basal force induced by flows with different particle sizes and Froude numbers are compared in Figure 4a and Figure 4b, respectively. The probability of basal

normal forces decays with an increasing normalized basal force. Similar distribution of the normalized basal force was also observed by McCoy *et al.* (2013) in their field measurements. It is evident that the basal forces fluctuate more significantly from their moving average as the particle size and the flow Froude number increase. In Figure 4(a), the weighted average value of the normalized basal forces with a positive fluctuation are calculated to be 1.03, 1.19 and 1.55 for experiments carried with flow particles of 1.5, 7 and 11 mm, respectively. In Figure 4(b), the weighted average of the normalized basal forces with a positive fluctuation are calculated to be 1.30, 1.46, and 1.55 for experiments with Froude numbers of 3.6, 4.8, and 5.4, respectively. The increasing trend of the normalized basal forces with the flow particle size and Froude number exhibits a strong dependency on the boundary collisional stresses. This increasing trend agrees with equation (11) and implies that the flow particle size and the Froude number are the two governing parameters that determine the boundary collisional stresses and the erosion potential of flow-type landslides.

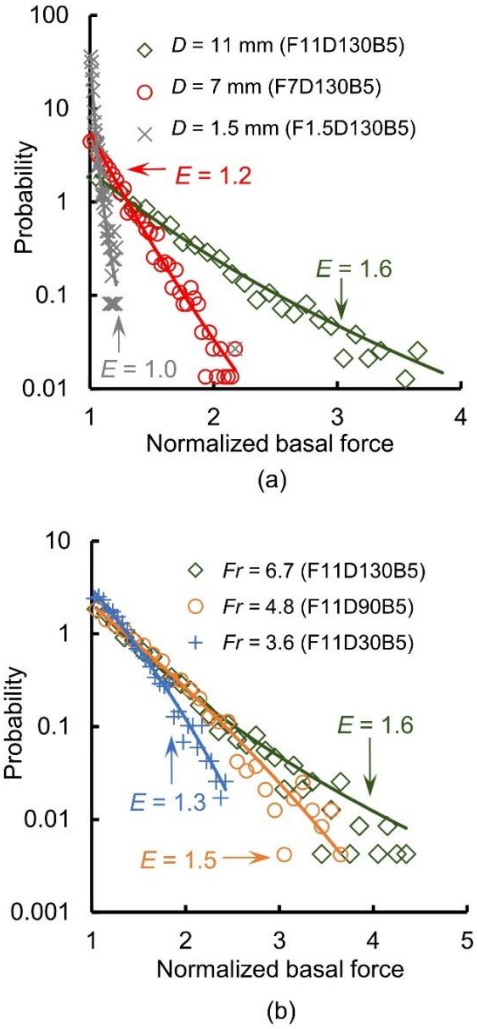

Figure 4. Probability distribution of the measured basal forces with a positive fluctuation generated by flows with different particle sizes (a) and Froude number (b) in the test F11D130B5 (D = 11 mm, Fr = 6.7, θ = 5%)

Table 3. Summary of experiment results

Test ID	Representative flow velocity, v (m/s)	Representative flow height, h (mm)	Froude number, Fr	Soil strength, c_u (Pa)	Erosion potential, N_c	Erosion depth, e (mm)	Erosion rate, $\dot{e}$ (mm/s)
F11D130B5	2.9	19.3	6.7	985	0.36	15.1	6.7
F9D130B5	3.0	18.3	7.0	950	0.29	11.4	4.1
F7D130B5	3.0	18.9	6.9	905	0.24	9.9	3.6
F4D130B5	2.8	18.3	6.6	1001	0.11	5.6	2.5
F1.5D130B5	2.7	18.8	6.2	954	0.05	1.3	0.4
F0.2D130B5	2.5	21.3	5.4	967	0.01	0.1	0.02
F11D110B5	2.7	22.6	5.7	981	0.35	12.6	6.3
F11D90B5	2.4	25.8	4.8	947	0.34	11.3	5.5
F11D70B5	2.3	26.1	4.6	961	0.33	10.7	5.6
F11D50B5	2.2	29.7	4.0	1010	0.30	8.2	4.8
F11D30B5	2.0	32.3	3.6	1004	0.29	7.4	4.7
F4D130B28	2.9	21.3	6.3	1726	0.06	3.6	0.8
F4D130B25	2.9	20.7	6.5	1576	0.07	2.6	0.5
F4D130B20	3.0	21.8	6.6	1321	0.08	2.6	0.5
F4D130B17	2.9	19.6	6.5	1239	0.09	3.3	0.8
F4D130B13	3.0	20.4	6.7	1071	0.10	4.5	0.9
F4D130B10	3.0	20.8	6.7	992	0.11	4.9	1.5

Note: [a]In the test ID, F represents the flow particle size, D represents the distance between the gate and the erodible bed, and B represents the volumetric bed water content

[b]Basic properties of Toyoura sand reported by Unno et al. (2008) and Ishihara (1993) are used to estimate the soil strength

[c]The average flow front velocity on the erodible bed is chosen as the representative flow velocity. The representative Froude number is calculated with the representative velocity according to Equation (11b)

333 **Table 4.** Erosion depth measured by the erosion columns

Test ID	Erosion depth, e: mm													
	l = 30 mm	l = 85 mm	l = 140 mm	l = 195 mm	l = 250 mm	l = 305 mm	l = 360 mm	l = 415 mm	l = 470 mm	l = 525 mm	l = 580 mm	l = 635 mm	l = 690 mm	l = 745 mm
F11D130B5	11.6	31.9	43.1	42.9	37.7	9.95	1.25	2.2	2.2	2.95	4.9	6.35	7.6	8.6
F9D130B5	3.9	23.2	40.1	42.7	16.8	4.9	2.5	1.5	1.5	1.0	4.0	5.4	6.3	5.4
F7D130B5	3.0	16.2	39.3	31.4	8.6	0.5	0.5	2.0	0.7	2.0	5.2	5.9	5.3	4.4
F4D130B5	4.9	26.1	13.0	1.0	0.7	0.0	0.5	4.4	10.5	6.8	5.2	2.2	2.2	1.0
F1.5D130B5	10.3	0.5	0.0	0.0	0.0	2.5	3.5	0.5	0.5	0.0	0.0	0.0	0.0	0.0
F0.2D130B5	0.0	0.0	0.0	0.0	0.0	0.0	0.0	0.0	0.0	0.0	0.5	0.0	0.5	0.0
F11D110B5	14.8	33.5	42.7	35.5	10.2	2.2	5.1	3.2	2.9	3.0	3.4	5.9	7.1	7.3
F11D90B5	16.6	30.0	38.3	21.1	5.6	2.9	4.9	3.9	4.9	5.6	5.1	5.3	7.4	6.8
F11D70B5	17.4	32.2	37.2	23.3	6.6	1.0	3.2	2.9	1.5	6.7	5.4	3.4	3.4	6.3
F11D50B5	19.7	27.4	16.6	6.1	2.0	4.5	5.9	4.2	4.0	4.4	4.5	3.5	6.3	6.4
F11D30B5	21.5	32.3	11.8	2.9	2.4	2.2	2.4	3.9	3.9	3.9	4.4	2.5	4.9	4.4
F4D130B28	11.3	12.6	0.0	0.0	0.0	1.0	6.1	3.4	3.9	3.9	2.0	3.4	1.2	1.5
F4D130B25	6.4	19.2	0.0	0.0	0.0	0.0	0.0	0.7	1.5	0.0	5.4	2.4	0.0	0.0
F4D130B20	5.4	18.9	0.0	0.0	0.0	0.0	0.0	0.0	3.4	3.5	2.9	1.5	0.5	0.0
F4D130B17	3.9	21.5	1.5	0.0	0.0	0.0	0.0	1.5	4.7	2.5	2.9	5.6	1.9	0.0
F4D130B13	4.0	24.1	3.9	0.0	0.0	0.5	0.0	0.5	4.9	7.4	7.4	3.5	4.4	1.9
F4D130B10	3.5	22.7	19.9	0.5	0.0	0.5	0.0	0.0	0.0	5.9	7.9	7.3	0.5	0.0
F11D130B5	8.8	30.5	40.9	40.3	38.3	11.7	2.0	3.4	4.4	3.0	6.4	7.8	8.4	9.3

334
335

336 **Table 5.** Experiment results of bedrock erosion obtained by Hsu et al. (2008)

Test ID	Flow particle size, D: mm	Drum Velocity, u_d: m/s	Flow surface Velocity, u_f: m/s	Flow depth, h_f: mm	Froude number, Fr	Tensile strength, τ: kPa	Erosion potential, N_{CR}	Erosion rate, $\dot{e}$: 10^{-3} mm/s
1	10	0.78	0.4	60	1.54	814	0.55	1.57
2	10	0.78	0.4	85	1.29	814	0.50	1.21
3	10	0.31	0.4	55	0.97	814	0.42	0.42
4	10	0.28	0.4	90	0.72	814	0.36	0.31
5	4	0.79	0.4	50	1.70	814	0.23	0.76
6	4	0.54	0.4	50	1.34	814	0.20	0.33
7	6	0.53	0.4	60	1.21	592	0.55	0.57
8	4	0.53	0.4	60	1.21	592	0.36	0.32
9	10	0.53	0.4	65	1.16	592	0.89	1.61
10	1	0.52	0.4	40	1.47	592	0.10	0.00
11	4	0.77	0.5	50	1.81	592	0.46	0.25
12	1	0.52	0.4	40	1.47	407	0.21	0.28
13	1	0.7	0.4	40	1.76	407	0.24	0.32
14	10	0.52	0.4	65	1.15	407	1.87	7.20
15	4	0.52	0.5	50	1.46	407	0.85	1.99
16	6	0.52	0.4	60	1.20	407	1.15	4.78
17	4	0.77	0.5	50	1.81	653	0.37	0.61

337
338
339

4.2 Effects of flow particle size and Froude number on soil bed erosion

Figure 5 shows the effects of the flow particle size on the soil bed erosion rate. The erosion rate increases linearly with the flow particle size. Figure 4(a) shows that the boundary collisional stresses increase with flow particle size. Consequently, the erosion potential and the erosion rate also increase. For the experiment conducted with a flow particle size of 0.2 mm, minor basal force fluctuation is observed and the measured basal force is approximately equal to the overburden of the flow because the boundary collisional stresses are negligible compared to the frictional shear stress. A measured erosion rate of 0.02 mm/s with a particle size of 0.2 mm agrees with the previous demonstration whereby the frictional shear stress is insufficient to erode an unsaturated soil bed. This is because the soil strength mobilized by the overburden and the soil strength provided by matric suction counteract the induced frictional shear stress. Thus, the erosion potential of flow-type landslides on a soil bed can be predicted solely with the boundary collisional stresses.

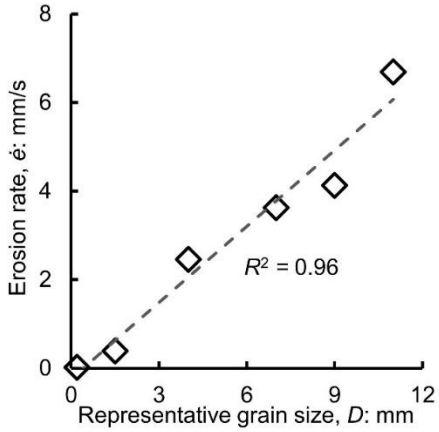

Figure 5. Effects of flow particle size on the erosion rate of unsaturated soil bed

In this study, the Froude number of the experimental flows is varied over a broad range from 3.6 to 7.0 to verify the increasing trend of erosion with the Froude number. Equation (15) dictates that the erosion rate of flow-type landslides follows a power-law relationship with the Froude number. However, theoretical analysis can only provide the range of the power-law coefficient. The lower bound of the power-law coefficient is 0. A power-law coefficient of 2 is the upper bound whereby the particle collisions are perfectly elastic. However, the experiment results in Table 3 show that the erosion rate increases with the Froude number, which agrees with Equation (15).

Figure 6(a) shows the correlation between the proposed erosion potential N_c and the soil bed erosion rate $\dot{e}$ with a power-law coefficient of 0.2, which yields the best linear fit with the experimental data. A power-law coefficient of 0.2 is between the upper and lower bounds and implies that the collisions between the flow particles and the soil bed are inelastic. It is worthwhile to note that the trend line intersects the x-coordinate (i.e., erosion potential) at $N_C = 0.045$. The intersection 0.045 is the minimum erosion potential required for the boundary collisional stresses to erode the soil bed material in this study.

Figure 6(b) shows the correlation between the erosion rate and the strength normalized collisional stresses N_{SNCS} (Song & Choi, 2021). A general observation is that the correlation coefficient between the erosion rate and N_{SNCS} is lower than that between the erosion rate and N_{C}. N_{SNCS} is defined based on the inter-particle collisional stresses within the flow, while N_{C} is defined based on the boundary collisional stresses by considering the basal slip velocity. Therefore, N_{C} yields a more accurate representation of the erosion potential of flow-type landslides compared to N_{SNCS}.

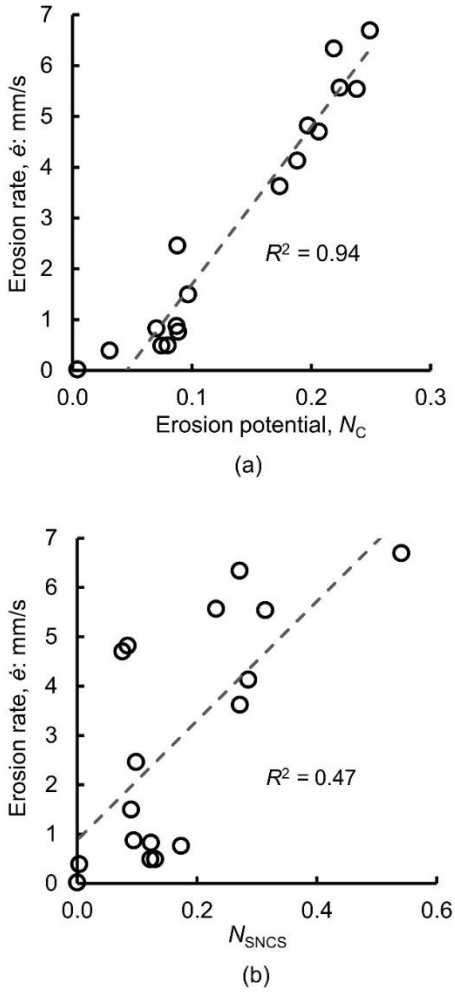

Figure 6. Correlation between the erosion rate and (a) the N_{C} and (b) the N_{SNCS} defined by Song & Choi (2021)

4.3 Effects of boundary collisional stresses on the erosion of rock bed

Research in the literature shows that the dominant mechanism of rock bed erosion is also collisional stresses (Stock & Dietrich, 2006; Hsu *et al.*, 2008), and the failure of rock is governed by T^2/E_{ff}, where T is the tensile strength and E_{ff} is the Young's modulus (Jaeger *et al.*, 2009). However, existing theories neglect the effects of basal slip condition when representing the driving mechanism of rock erosion.

Based on the above derivation of boundary collisional stresses, the erosion potential of flow-type landslides on a rock bed N_{CR} can be expressed as:

$$N_{\mathrm{CR}} = \frac{\sigma_{\mathrm{bc}}}{T^2/E_{\mathrm{ff}}} = \frac{\chi g \nu_{\mathrm{f}} \rho_{\mathrm{s}} D F r^{2k}}{T^2/E_{\mathrm{ff}}} \quad (16)$$

The rock erosion rate should be dependent on the N_{CR}. Equation (16) can be evaluated by using the experiment data obtained by Hsu *et al.* (2008), where the erosion of rock by granular flow in a 0.56-m rotating drum was simulated. A summary of the test results is shown in Table 5. Figure 7 shows the correlation between the erosion rate and N_{CR}. The data points collapse on a linear trend line with a high correlation coefficient of 0.91 if a power-law coefficient of 0.56 is adopted. The linear correlation between the erosion rate of a rock bed and the erosion potential defined by equation (16) shows that the boundary collisional stresses (equation (11)) are properly formulated. This implies that it may be possible to unify the theories of bedrock erosion and soil bed erosion. This finding can facilitate an improved understanding of the evolution of the geomorphology in mountainous settings by flow-type landslides.

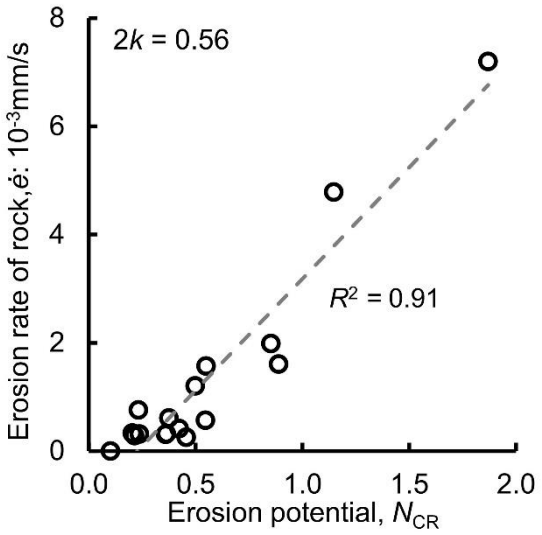

Figure 7. Correlation between the erosion rate of rock bed and the N_{CR}

4.4 Implications on the modelling of flow-type landslides

This study shows that existing erosion models do not explicitly capture the role of basal slip velocity on the boundary collisional stresses and the effects of the volumetric response on the unsaturated soil bed strength. The conventional models are a gross simplification of the actual phenomenon, and such idealizations will limit advancement towards the replication of field observation. The newly-proposed model (equation (15)) shows that both the boundary collisional stresses and the erosion of soil bed increase with the flow particle size and Froude number. Therefore, future research work that improves the estimation of the characteristic flow particle size and Froude number is critical for vulnerability

assessments of flow-type landslides. There is a pressing need to advance non-invasive methods (i.e., Kanellakis & Nikolakopoulos, 2017) for realistic estimation of the potential particle size distribution of the debris material. Furthermore, to model the correct volumetric response and the mobilized strength due to the volumetric contraction under landslide loading, it is evident that prior knowledge of the antecedent bed water conditions is required.

This research aimed to mimic soil bed erosion at the front of flow-type landslides, where solid stresses (i.e., frictional and collisional) dominate the erosion process. Recent field observations (De Haas et al., 2022, McCoy et al., 2012) show that the fluidized body and tail of the flow, where the fluid stress dominate the flow dynamics, also contribute to soil bed erosion. The fluid shear stress is not determined by flow overburden but by flow velocity (Zagarola & Smits, 1998). Furthermore, the mobilized soil strength caused by overburden may not entirely counteract the fluid shear stresses imposed by the flow body or tail. Moreover, the infiltration of fluid into an unsaturated soil bed will destroy the matric suction and reduce the soil bed strength. Evidently, fluid stresses may also play a significant role in soil bed erosion.

5. CONCLUSIONS

The mechanics of soil bed erosion is investigated and a new model of the erosion potential of flow-type landslides is proposed. A total of 17 physical experiments were carried to evaluate the newly proposed model. Conclusions may be drawn as follows:

- When subjected to landslide loading, the volume contraction of unsaturated soil due to the compressibility of the air phase mobilizes shear strength, which counteracts the induced frictional shear stress by the flow overburden. Consequently, frictional shear stress alone is insufficient to erode unsaturated soil beds. The finding highlights the importance of considering unsaturated soil mechanisms in assessments of soil bed erosion caused by flow-type landslides. It is evident that the assumption of saturated soil bed in existing theories is unrealistic. Furthermore, the finding implies that the assumption of friction-driven soil bed erosion, which existing models are based on, does not constitute the dominant driving mechanism correctly and requires further evaluation.

- Boundary collisional stresses govern the erosion of unsaturated soil beds, and the erosion potential of the flow-type landslides can be quantified with the ratio of boundary collisional stresses to the unsaturated soil strength. Both the boundary collisional stresses and the erosion rate of the soil bed increase linearly with the flow particle size and demonstrates a power-law relationship with the Froude number. This finding reveals the importance of the effects of flow particle size and the Froude number on the assessment of soil bed erosion. Further, this study highlights the need for non-invasive method (e.g., remote sensing and computer vision) to estimate the particle size of the debris materials on the slopes for the assessment of erosion potential of the potential flow-type landslides.

- Boundary collisional stresses dominate the erosion of both rock and soil beds, and the theories of rock erosion and soil bed erosion can be unified with the dimensionless number defined as the ratio of boundary collisional stresses to the strength of the bed material. The unified theory can facilitate the modelling of the evolution of the geomorphology of the mountains and the evolution of flow-type landslides in the field, where there is hybrid of rock bed and soil bed.

Acknowledgements

The authors are grateful for the generous financial sponsorship from the Research Grants Council of Hong Kong (General Research Fund Grants 16210219; AoE/E-603/18). The authors declare no financial conflicts of interests.

References:

Artoni, R., Santomaso, A. C., Go, M. & Canu, P. (2012). Scaling Laws for the Slip Velocity in Dense Granular Flows. *Phys. Rev. Lett.* **108**, No. 23, 238002, https://doi.org/10.1103/PhysRevLett.108.238002.

Bagnold, R. A. (1954). Experiments on a gravity-free dispersion of large solid spheres in a Newtonian fluid under shear. *Proc. Math. Phys. Eng.* ***225***, No. 1160, 49-63, https://doi.org/10.1098/rspa.1954.0186.

Berger, C., McArdell, B. W. & Schlunegger, F. (2011). Direct measurement of channel erosion by debris flows, Illgraben, Switzerland. *J. Geophys. Res.-Earth Surface* **116**, No. F1, F01002, https://doi.org/10.1029/2010JF001722

Coe, J. A., Kinner, D. A. & Godt, J. W. (2008). Initiation conditions for debris flows generated by runoff at Chalk Cliffs, central Colorado. *Geomorphology* **96**, No. 3-4, 270-297, https://doi.org/10.1016/j.geomorph.2007.03.017.

De Haas, T., McArdell, B.W., Nijland, W., Åberg, A.S., Hirschberg, J. & Huguenin, P. (2022). Flow and Bed Conditions jointly control Debris-Flow Erosion and Bulking. *Geophys. Res. Lett.*, ***49***, e2021GL097611, https://doi.org/10.1029/2021GL097611.

Farin, M., Tsai, V. C., Lamb, M. P. & Allstadt, K. E. (2019). A physical model of the high-frequency seismic signal generated by debris flows. *Earth. Surf. Proc. Land.* **44**, No. 13, 2529-2543, https://doi.org/10.1002/esp.4677.

Fredlund, D. G., Morgenstern, N. R. & Widger, R. A. (1978). The shear strength of unsaturated soils. *Can. Geotech. J.* **15**, No. 3, 313-321, https://doi.org/10.1139/t78-029.

Fredlund, D. G. & Rahardjo, H. (1993). *Soil mechanics for unsaturated soils*. John Wiley & Sons.

GEO (2017). 3D Debris Mobility Assessment Using LS-DYNA. *GEO Report*, No. 325

Hilf, J. W. (1948). Estimating construction pore pressures in rolled earth dams. In *Proc. 2nd Int. Conf. Soil Mech. Found. Eng.* Rotterdam, The Netherlands, Vol. 3, pp. 234-240.

Hsu, L., Dietrich, W. E. & Sklar, L. S. (2008). Experimental study of bedrock erosion by granular flows. *J. Geophys. Res. - Earth Surface* **113**, No. F2, F02001, https://doi.org/10.1029/2007JF000778.

Hsu, L., Dietrich, W. E. & Sklar, L. S. (2014). Mean and fluctuating basal forces generated by granular flows: Laboratory observations in a large vertically rotating drum. *J. Geophys. Res. – Earth Surface* **119**, No. 6, 1283-1309, https://doi.org/10.1002/2013JF003078.

494 Hungr, O. & Evans, S. G. (2004). Entrainment of debris in rock avalanches: An analysis of a long run-out
495 mechanism. *Geol. Soc. Am. Bull.* **116**, No. 9-10, 1240-1252, https://doi.org/10.1130/B25362.1.
496 Hungr, O., Leroueil, S. & Picarelli, L. (2014). The Varnes classification of landslide types, an update.
497 *Landslides* **11**, No. 2, 167-194, https://doi.org/10.1007/s10346-013-0436-y.
498 Iverson, R. M. (1997). The physics of debris flows. *Rev. Geophys.* **35**, No. 3, 245-296,
499 https://doi.org/10.1029/97RG00426.
500 Iverson, R. M. (2012). Elementary theory of bed-sediment entrainment by debris flows and avalanches. *J.*
501 *Geophys. Res. – Earth Surface* **117**, No. F3, F03006 , https://doi.org/10.1029/2011JF002189.
502 Iverson, R. M. (2015). Scaling and design of landslide and debris-flow experiments. *Geomorphology* **244**,
503 9-20, https://doi.org/10.1016/j.geomorph.2015.02.033.
504 Jaeger, J. C., Cook, N. G. & Zimmerman, R. (2009) *Fundamentals of rock mechanics*. John Wiley &
505 Sons.
506 Jerolmack, D. J. & Daniels, K. E. (2019). Viewing Earth's surface as a soft-matter landscape. *Nat. Rev.*
507 *Phys.* **1**, No. 12, 716-730, https://doi.org/10.1038/s42254-019-0111-x.
508 Kanellakis, C. & Nikolakopoulos, G. (2017). Survey on Computer Vision for UAVs: Current
509 Developments and Trends. *J. Intell. Robot. Syst.* **87**, No. 1, 141-168, https://doi.org/10.1007/s10846-017-
510 0483-z.
511 Kwan, J. S. H., Koo, R. C. H. & Ng, C. W. W. (2015). Landslide mobility analysis for design of multiple
512 debris-resisting barriers. *Can. Geotech. J.* **52**, No. 9, 1345-1359, https://doi.org/10.1139/cgj-2014-0152.
513 Lang, M., Guo, H., Odegard, J. E., Burrus, C. S. & Wells, R. O. (1996). Noise reduction using an
514 undecimated discrete wavelet transform. *IEEE Signal Proc. Lett.* **3**, No. 1, 10-12,
515 https://doi.org/10.1109/97.475823.
516 McArdell, B. W., Bartelt, P. & Kowalski, J. (2007). Field observations of basal forces and fluid pore
517 pressure in a debris flow. *Geophys. Res. Lett.* **34**, No. 7, L07406, https://doi.org/10.1029/2006GL029183.
518 McCoy, S. W., Kean, J. W., Coe, J. A., Tucker, G. E., Staley, D. M., et al. (2012). Sediment entrainment
519 by debris flows: In situ measurements from the headwaters of a steep catchment. *J. Geophys. Res. – Earth*
520 *Surface* **117**, No. F3, F03016, https://doi.org/10.1029/2011JF002278
521 McCoy, S. W., Tucker, G. E., Kean, J. W. & Coe, J. A. (2013). Field measurement of basal forces
522 generated by erosive debris flows. *J. Geophys. Res. – Earth Surface* **118**, No. 2, 589-602,
523 https://doi.org/10.1002/jgrf.20041
524 McDougall, S. & Hungr, O. (2005). Dynamic modelling of entrainment in rapid landslides. *Can. Geotech.*
525 *J.* **42**, No. 5, 1437-1448, https://doi.org/10.1139/t05-064.
526 Pirulli, M. & Pastor, M. (2012). Numerical study on the entrainment of bed material into rapid landslides.
527 *Geotechnique* **62**, No. 11, 959-972, https://doi.org/10.1680/geot.10.P.074.
528 Skempton, A. W. (1954). The pore-pressure coefficients A and B. *Geotechnique*, **4**, No. 4, 143-147,
529 https://doi.org/10.1680/geot.1954.4.4.143
530 Sklar, L. S. & Dietrich, W. E. (2001). Sediment and rock strength controls on river incision into bedrock.
531 *Geology* **29**, No. 12, 1087-1090, https://doi.org/10.1130/0091-7613(2001)029<1087:SARSCO>2.0.CO;2.

Song, P. J. & Choi, C. E. (2021). Revealing the Importance of Capillary and Collisional Stresses on Soil Bed Erosion Induced by Debris Flows. *J. Geophys. Res. – Earth Surface* **126**, No. 5, https://doi.org/10.1029/2020JF005930.

Stock, J. D. & Dietrich, W. E. (2006). Erosion of steepland valleys by debris flows. *Geol. Soc. Am. Bull.* **118**, No. 9-10, 1125-1148, https://doi.org/10.1130/B25902.1.

Takahashi, T. (1978). Mechanical Characteristics of Debris Flow. *J. Hydr. Eng. Div.* **104**, No. 8, 1153-1169, https://doi.org/10.1061/JYCEAJ.0005046.

Yohannes, B., Hsu, L., Dietrich, W. E. & Hill, K. M. (2012). Boundary stresses due to impacts from dry granular flows. *J. Geophys. Res. - Earth Surface* **117**, No. F2, F02027, https://doi.org/10.1029/2011JF002150.

Zagarola, M. V. & Smits, A. J. (1998). Mean-flow scaling of turbulent pipe flow. *J. Fluid Mech.* 373, 33-79, https://doi.org/10.1017/S0022112098002419.

Zhou, G. G. D., Hu, H. S., Song, D., Zhao, T. & Chen, X. Q. (2019). Experimental study on the regulation function of slit dam against debris flows. *Landslides* **16**, No. 1, 75-90, https://doi.org/10.1007/s10346-018-1065-2.

Zhou, G. G., Cui, K. F., Jing, L., Zhao, T., Song, D. and Huang, Y. (2020). Particle size segregation in granular mass flows with different ambient fluids. *J. Geophys. Res. - Solid Earth*, **125**, No. 10, e2020JB019536, https://doi.org/10.1029/2020JB019536.